online data

# NMR structure of bucandin, a neurotoxin from the venom of the Malayan krait (*Bungarus candidus*)

Allan M. TORRES*, R. Manjunatha KINI†, Nirthanan SELVANAYAGAM‡ and Philip W. KUCHEL*[1]

*Department of Biochemistry, University of Sydney, N. S. W. Australia 2006, †Department of Biological Sciences, Faculty of Science, National University of Singapore, 10 Kent Ridge Crescent, Singapore 119260, and ‡Department of Anatomy, Faculty of Medicine, National University of Singapore, 10 Kent Ridge Crescent, Singapore 119260

A high-resolution solution structure of bucandin, a neurotoxin from Malayan krait (*Bungarus candidus*), was determined by $^1$H-NMR spectroscopy and molecular dynamics. The average backbone root-mean-square deviation for the 20 calculated structures and the mean structure is 0.47 Å (1 Å = 0.1 nm) for all residues and 0.24 Å for the well-defined region that spans residues 23–58. Secondary-structural elements include two antiparallel $\beta$-sheets characterized by two and four strands. According to recent X-ray analysis, bucandin adopts a typical three-finger loop motif and yet it has some peculiar characteristics that set it apart from other common $\alpha$-neurotoxins. The presence of a fourth strand in the second antiparallel $\beta$-sheet had not been observed before in three-finger toxins, and this feature was well represented in the NMR structure. Although the overall fold of the NMR structure is similar to that of the X-ray crystal structure, there are significant differences between the two structures that have implications for the pharmacological action of the toxin. These include the extent of the $\beta$-sheets, the conformation of the region spanning residues 42–49 and the orientation of some side chains. In comparison with the X-ray structure, the NMR structure shows that the hydrophobic side chains of Trp$^{27}$ and Trp$^{36}$ are stacked together and are orientated towards the tip of the middle loop. The NMR study also showed that the two-stranded $\beta$-sheet incorporated in the first loop, as defined by residues 1–22, and the C-terminus from Asn$^{59}$, is probably flexible relative to the rest of the molecule. On the basis of the dispositions of the hydrophobic and hydrophilic side chains, the structure of bucandin is clearly different from those of cytotoxins.

Key words: four-stranded anti-parallel $\beta$-sheet, molecular dynamics, snake venom, solution structure, three-finger toxin.

## INTRODUCTION

The 'three-finger' loop motif is a common structural feature shared by a family of polypeptide toxins present in many snake venoms. These highly potent toxins are usually 60–75 amino acid residues in length and incorporate 4 or 5 disulphide bridges that stabilize their tertiary structure. Their structures are also characterized by the presence of an anti-parallel $\beta$-sheet that spans two neighbouring loops. Despite similarities in overall fold, three-finger toxins have diverse pharmacological functions. Members of this group include $\alpha$-neurotoxins that block acetylcholine receptors [1–3], cardiotoxins that damage cell membranes [4–6], fasciculins that inhibit acetylcholine esterase [7] and L-type calcium-channel blockers [8,9].

Bucandin is a novel neurotoxin recently isolated from the venom of the Malayan krait (*Bungarus candidus*). This 63-amino-acid polypeptide enhances the release of acetylcholine from nerve terminals and belongs to a family of three-finger toxins that incorporate five disulphide bridges. Its amino acid sequence has only 30–40 % sequence identity with many three-finger toxins, but it is quite similar to S6C4 toxin from *Dendroaspis jamesonii kaimosae* [a subspecies of *D. jamesonii* (Jameson's mamba)] in which 67 % of the amino acid residues are identical.

The structure and pharmacological effects of bucandin are of considerable interest in defining the mode of action of the venom and its possible pharmaceutical uses. The recent atomic-resolution X-ray structure of bucandin shows a highly polar molecule that incorporates two anti-parallel $\beta$-sheets [10]. The first loop is isolated from the rest of the molecule, with the tip of the loop twisted away from the rest of the molecule. In the present paper we report a high-resolution structure of bucandin obtained by NMR, as well as details of its separation and purification. The NMR structure is compared in detail with the X-ray structure and with other known three-finger toxins. Additional information on the molecular-dynamical behaviour of bucandin in solution is also presented.

## MATERIALS AND METHODS

### Materials

Freeze-dried *Bungarus candidus* venom was obtained from Venom Supplies (Tanunda, SA, Australia). Prepacked columns, Superdex 30 and Nucleosil $C_{18}$ were purchased from Pharmacia Biotech (Uppsala, Sweden) and Phenomenex (Torrance, CA, U.S.A.) respectively. Reagents for N-terminal amino acid sequencing were from Applied Biosystems (Foster City, CA, U.S.A.). The chromatographic reagents, acetonitrile and TFA were from Fisher Scientific (Fair Lawn, NJ, U.S.A.) and Fluka

Abbreviations used: DQF-COSY, double-quantum-filtered scalar COSY; ECOSY, exclusive COSY; NOE, nuclear Overhauser enhancement; RMSD, root-mean-square deviation; 1D, one-dimensional; 2D, two-dimensional; TFA, trifluoroacetic acid.

[1] To whom correspondence should be addressed (e-mail p.kuchel@biochem.usyd.edu.au).

The protein sequence data reported in this paper have been deposited in the SWISS-PROT Protein Data Bank under the accession number P81782. The $^1$H-chemical-shift assignments have been deposited in BioMagRes Bank under the accession number 5097 and are also available online at http://www.BiochemJ.org/bj/360/bj3600539add.htm (one table). The co-ordinates of the ensemble of 20 structures have been deposited in the Research Collaboratory for Structural Bioinformatics ('RSCB') Protein Data Bank (PDB) under the accession code 1IJC.

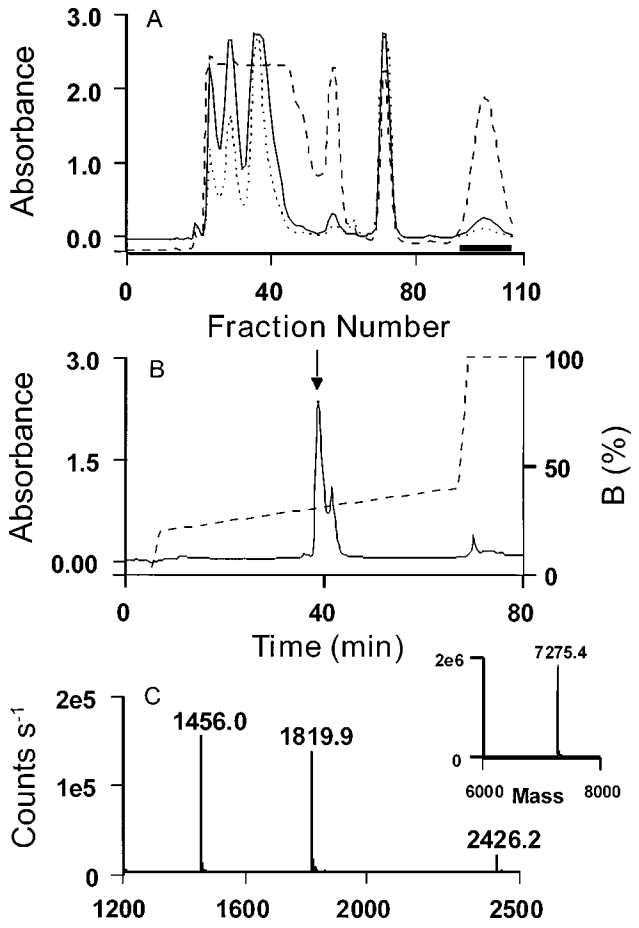


**Figure 1 Purification of bucandin**

(**A**) Gel-filtration chromatography of *Bungarus candidus* venom (150 mg) on a Superdex 30 FPLC column (1.6/60) column. The column was equilibrated and eluted with 50 mM Tris/HCl buffer, pH 7.4, at a flow rate of 1.5 ml/min. The continuous line represents the absorbance at 280 nm, the broken line that at 215 nm and dotted line that at 254 nm. The fraction size was 2 ml. (**B**) The last peak (indicated by the horizontal bar) from gel-filtration chromatography was further purified on a reverse-phase Nucleosil $5C_{18}$ (2 cm × 25 cm) column equilibrated with 0.1% (v/v) TFA, and the bound proteins were eluted with a linear gradient of 80% (v/v) acetonitrile in 0.1% (v/v) TFA at a flow rate of 2 ml/min. Bucandin was isolated from the peak indicated by the arrow. (**C**) Electrospray-ionisation MS of bucandin. The spectrum shows a series of multiply charged ions, corresponding to a single, homogeneous peptide of molecular mass 7275.4 (inset).

(Buchs, Switzerland) respectively. All other chemicals used were of analytical reagent grade.

### Isolation and purification of bucandin

Whole venom (150 mg) was dissolved in 1 ml of MilliQ water and centrifuged at 3000 ***g*** for 5 min. The crude venom supernatant was fractionated, on the basis of the molecular masses of the components, on a Superdex 30 FPLC column (1.6 cm × 60 cm), using 50 mM Tris/HCl buffer, pH 7.5, at a flow rate of 1.5 ml/min as eluent. The last peak, containing bucandin, was further purified on a reverse-phase Nucleosil 5 $C_{18}$ column (2 cm × 25 cm). The column was equilibrated with 0.1% (v/v) TFA, and the bound proteins were eluted with a linear gradient of 80% acetonitrile in 0.1% (v/v) TFA at a flow rate of 2 ml/min.

### Electrospray MS

Bucandin was dissolved in acetonitrile/water (1:1, v/v) and analysed using a Perkin–Elmer Sciex API 300 triple quadrupole instrument, equipped with an ionspray interface. The ionspray voltage was set at 4600 V and the orifice voltage at 30 V. Nitrogen was used as a curtain gas with a flow rate of 0.6 litres/min, and compressed air was used as the nebulizer gas. The sample was infused into the mass spectrometer at a flow rate of 5 $\mu$l/min.

### Reduction and pyridylethylation

Bucandin was resuspended in 100 $\mu$l of the denaturant buffer (6.0 M guanidinium chloride/0.13 M Tris/1 mM EDTA, pH 8.0) containing 0.07 M $\beta$-mercaptoethanol. The solution was heated at 37 °C for 2 h. Subsequently, a 1.5-fold molar excess (over thiol groups) of 4-vinylpyridine was added and incubated at room temperature. After 2 h, the pyridylethylated sample was desalted by reverse-phase HPLC.

### N-terminal sequencing

N-terminal sequencing of the native and pyridylethylated protein was done by automated Edman degradation using a Procise 494 pulsed-liquid-phase protein sequencer (PerkinElmer–Applied Biosystems, Foster City, CA, U.S.A.) with an on-line 785A phenylthiohydantoin-amino acid analyser.

### NMR spectroscopy

The NMR sample was prepared by dissolving 4.3 mg of freeze-dried bucandin in 350 $\mu$l of $^1H_2O/^2H_2O$ (9:1) in a 5 mm Shigemi (Allison Park, PA, U.S.A.) tube. The resulting solution had a pH of 3.0, which is optimal for observing amide resonances. For the $^1H$–$^2H$ exchange experiment, the sample was freeze-dried and reconstituted in 350 $\mu$l of 99.6% $^2H_2O$; this sample was also used in other NMR experiments.

All NMR experiments were performed on a Bruker (Karlsruhe, Germany) AVANCE-600 DRX spectrometer using a 5 mm $^1H$ inverse probe with operating temperatures of 10, 25 or 35 °C. Two-dimensional (2D) NMR spectra were acquired in the phase-sensitive mode using time-proportional phase detection [11]. Homonuclear 2D spectra included double-quantum filtered (DQF-) COSY [12] with the phase-cycle modified for fast recycle times [13], ECOSY [14], TOCSY [15] with spin-lock period of 90 ms, and NOESY [16] with mixing times of 100 and 200 ms. Solvent signal-suppression was achieved either by using the WATERGATE pulse sequence [17] or by low-power irradiation at the water resonance frequency. A relaxation delay of 1.3 s between transients was employed in all 2D experiments.

$^1H$–$^2H$ exchange experiments were carried out by acquiring a series of 1D experiments for 1 h immediately after reconstituting the freeze-dried sample with $^2H_2O$. After this, five 1 h 2D TOCSY experiments were acquired to monitor further the rate of exchange, and to identify better the slowly exchanging amide protons. Backbone amide hydrogen-bond donors were identified as those that were slowly exchanging. Spectra were processed using XWIN-NMR software (Bruker).

### Structure calculations

Analysis of 2D spectra was performed using the XEASY program [18]. The NOESY spectrum recorded at 25 °C with a mixing time of 200 ms was chosen for the structural calculations. This ultimately provided 1258 non-redundant upper distance constraints for protons, based on the corresponding cross-peak

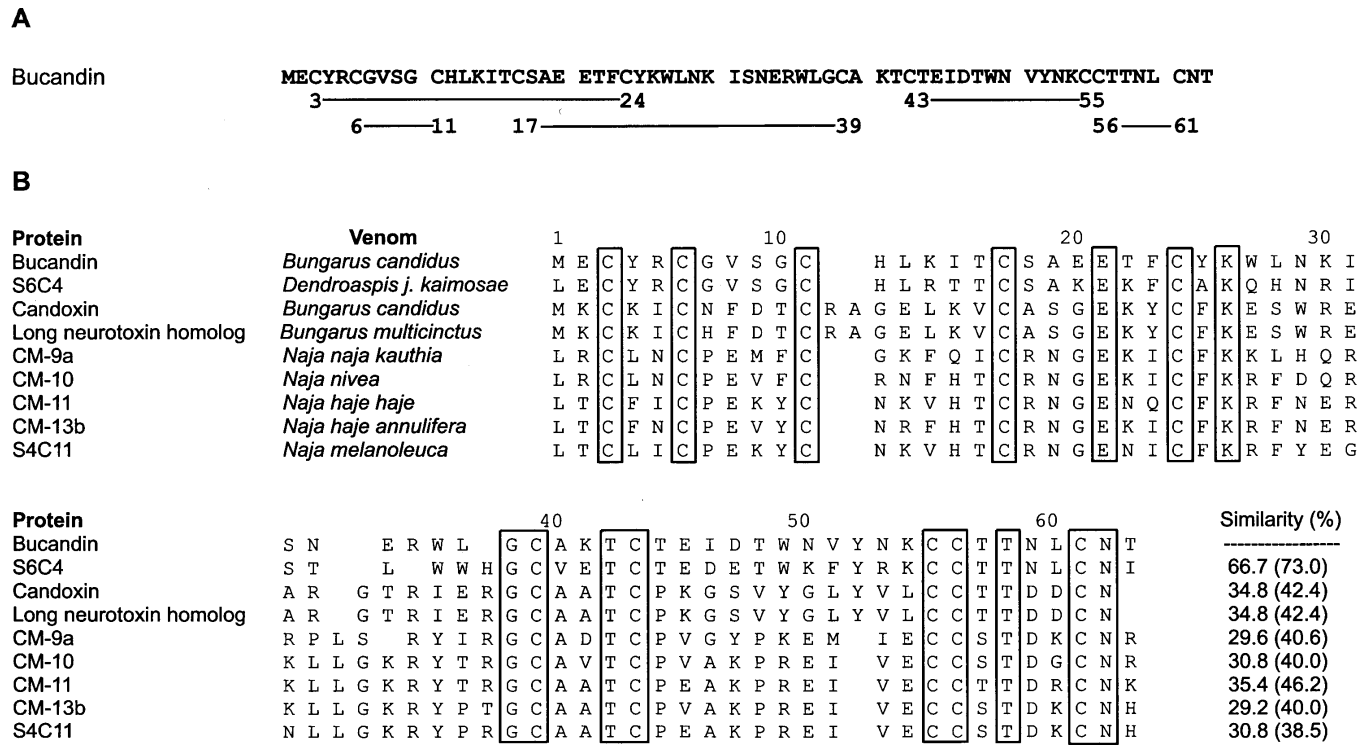


**Figure 2 Primary structures of bucandin and similar toxins**

(**A**) Amino acid sequence of bucandin and the disulphide-bonding pattern. (**B**) Sequence similarity between bucandin and other members of the small group of toxins containing the fifth disulphide in the first loop. Similarity values are given as percentage sequence identity and percentage sequence similarity (in parentheses).

intensities or volumes. A correction of 0.3 Å was added to all upper-distance bounds to allow for errors in spectral volume integration and conformational averaging.

Analysis of $^3J_{NH\alpha}$ coupling constants from 2D NOESY spectra, using the program INFIT [19], provided 45 $\phi$ dihedral angle constraints which were restrained as follows: $-120\pm30°$ for $^3J_{NH\alpha} = 8$–9 Hz and $-120\pm20°$ for $^3J_{NH\alpha} > 9$ Hz. $\chi_1$ Dihedral angle constraints and stereospecific assignments of methylene protons for some residues were obtained from the analysis of DQF-COSY, ECOSY and NOESY with 100 ms mixing time [20]. Deviations of $\pm30°$ were employed in all $\chi_1$ dihedral angle constraints which were set as either 180 or $-60°$.

Hydrogen-bonding pairs were deduced from $^1H$–$^2H$ exchange experiments, and the preliminary calculated structures. Hydrogen-bonding constraints were only introduced in the final stages of the structure calculations and were assigned upper distance-limits of 2.2 Å for $NH_i$ to $O_j$ and 3.2 Å for $N_i$ to $O_j$.

The NOAH protocol [21,22] in the torsion-angle dynamics program DYANA [23] was used in calculating preliminary structures and in assigning non-intra-residue and non-sequential NOESY cross-peaks. A few cycles of NOAH were used to obtain sufficient NOE constraints, after which the standard simulated annealing procedure in DYANA was applied. The disulphide linkages were identified from medium-resolution structures obtained after three rounds of NOAH calculations. These were found to be consistent with those identified earlier [10] and were used as additional constraints in the subsequent structure calculations. In the final structure calculations 6000 DYANA structures were generated from random starting conformations. The 'best' 120 structures defined as those with the lowest NOE violations, were then refined by simulated annealing with X-PLOR [24].

The simplified all-hydrogen force field was adopted, and the covalent geometry was constrained using the standard X-PLOR parameters. Details of the structure refinement procedure were given previously [24a].

## RESULTS

### Isolation and purification of bucandin

Bucandin was purified to homogeneity by a two-step method as follows. The crude *Bungarus candidus* venom was separated into seven fractions on a Superdex 30 gel-filtration column (Figure 1A). The last protein fraction was eluted after the salt volume of the column. The proteins in this peak were further fractionated on a reverse-phase HPLC column (Figure 1B). The major protein peak thus isolated was named bucandin. As shown in Figure 1(C), bucandin is homogeneous by electrospray-ionization MS. Bucandin has a molecular mass of $7275.43\pm0.32$ and constitutes about 2–3% of the crude venom.

### Amino acid sequence and structural similarity of bucandin

We were able to unequivocally identify all the residues and determine the complete amino acid sequence of both native (blank cycles where cysteine residues are found) and pyridylethylated bucandin samples. Bucandin has 63 amino acid residues, including ten cysteine residues (Figure 2A). The calculated mass is 7275.24. With an expected five disulphide bridges,

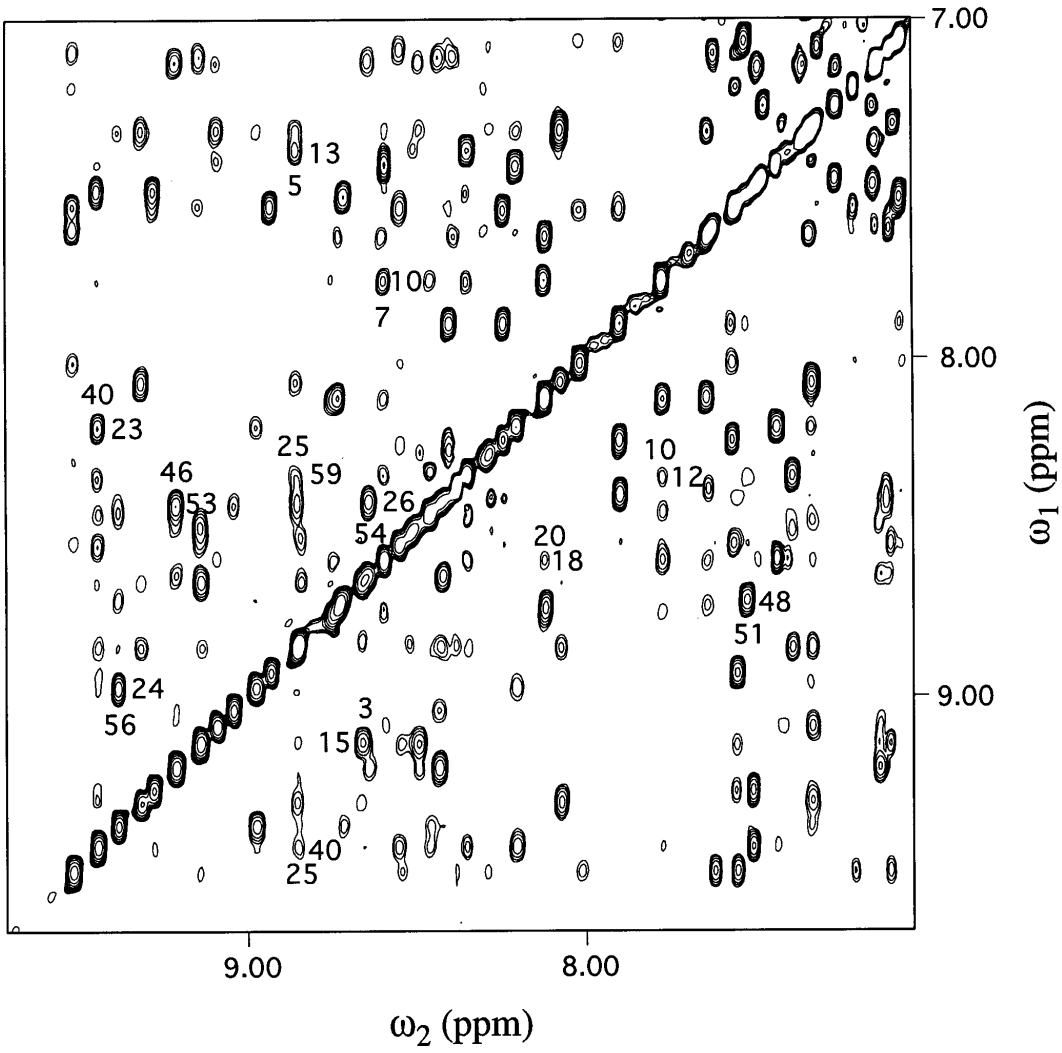


**Figure 3 Amide region of bucandin $^1$H NMR NOESY spectrum**

Selected medium- and long-range cross-peaks are labelled according to the order of the amino acid residue in the sequence. The 2D spectrum was obtained at 25 °C and pH 3.0.

the calculated mass of 7275.24 coincides well with the measured molecular mass of $7275.43 \pm 0.32$. Bucandin is similar to neurotoxins, cardiotoxins and other members of the three-finger toxin family. Unlike the most common members of this family, bucandin has the fifth disulphide bridge in the first loop. Figure 2(B) shows the sequence similarity between bucandin and other members of the small group of toxins containing the fifth disulphide in the first loop. Bucandin shows 73 % similarity to the $S_6C_4$ toxin from *D. j. kaimosae* venom. Most of the other toxins show a similarity of only 38–46 and an identity of only 28–35 %. About 15–16 % of similarity is due to ten cysteine residues and thus bucandin appears to be a novel protein.

### Structure determination by NMR

NMR assignments were made by using standard procedures [25]. Bucandin gave excellent 2D spectra with many cross-peaks that were well-dispersed, indicative that $\beta$-sheet structures were prevalent in the molecule. The quality of the spectra is exemplified by Figure 3, where the amide region of the 2D NOESY spectrum is shown. The assignment process was straightforward, since most of the proton resonances of bucandin at 298 K and pH 3.0 were well-resolved and narrow, although some of the peaks overlapped. Problems with the few amide proton peaks that overlapped were readily overcome by adjusting the temperature to give resolved peaks.

The NOAH automatic structure calculation scheme, with 24 cycles, provided highly folded structures that were of medium resolution. The obtained NOE constraints were then checked and were used as reference values in succeeding rounds of NOAH calculations; at this stage they included dihedral angle and hydrogen-bond constraints. After this, the simulated annealing procedure in DYANA was used to improve the quality of structures by performing an iterative cycle of calculation, structure analysis and constraint revision.

Final structural constraints consisted of 1258 non-redundant inter-proton distances from NOE, 61 dihedral angles and 44 hydrogen bond constraints. NOE constraints were composed of 466 long-range, 130 medium, 257 sequential and 405 intra-residue constraints. The best 120 out of 6000 structures generated in DYANA were subsequently refined by simulated annealing in X-PLOR. The best 20 structures with the lowest total energy

**Table 1 Structural statistics for the ensemble of 20 bucandin structures.**

Values are given as means ± S.D.

(a)

| Parameter | Value |
|---|---|
| Distance restraints | |
| Intra-residue ($i-j=0$) | 405 |
| Sequential ($\|i-j\|=1$) | 257 |
| Medium-range ($\|i-j\|\leqslant 5$) | 130 |
| Long-range ($\|i-j\|>5$) | 466 |
| Hydrogen bonds | 44 |
| Total | 1302 |
| Dihedral-angle restraints | |
| $\phi$ | 45 |
| $\chi_1$ | 16 |
| Mean RMS deviations from experimental restraints | |
| NOE (Å) | 0.0096 ± 0.0004 |
| Dihedrals (°) | 0.17 ± 0.04 |
| Mean RMS deviations from idealized covalent geometry* | |
| Bonds (Å) | 0.00091 ± 0.00004 |
| Angles (°) | 0.290 ± 0.002 |
| Impropers (°) | 0.114 ± 0.005 |
| Mean energies (kcal · mol$^{-1}$) | |
| $E_{NOE}$† | 6.05 ± 0.44 |
| $E_{cdih}$† | 0.11 ± 0.06 |
| $E_{vdW}$ | 0.10 ± 0.10 |
| $E_{bond}$ | 0.81 ± 0.06 |
| $E_{improper}$ | 1.04 ± 0.09 |
| $E_{angle}$ | 22.74 ± 0.27 |
| $E_{total}$ | 30.86 ± 0.68 |
| PROCHECK [26] Ramachandran plot analysis | |
| Most favoured region (%) | 65.4 |
| Additionally allowed region (%) | 30.9 |
| Generously allowed region (%) | 3.2 |
| Disallowed region (%) | 0.5 |

(b)

| | Atomic RMS differences (Å)‡ | |
|---|---|---|
| | Versus mean | Pairwise |
| Backbone atoms (23–58) | 0.24 ± 0.05 | 0.34 ± 0.07 |
| Heavy atoms (23–58) | 0.72 ± 0.07 | 1.01 ± 0.14 |

* Idealized geometry as defined by the CHARMM force field within X-PLOR.

† Final values of the square-well NOE and dihedral-angle potentials calculated with force constants of 50 kcal · mol$^{-1}$ · Å$^{-2}$ and 200 kcal · mol$^{-1}$ Å$^{-2}$ respectively.

‡ Atomic differences are given as average RMS difference against mean co-ordinate structure (mean) and average RMS difference of all pairwise structures (pairwise).

were considered as representatives of the bucandin structures. None of these structures had NOE violations greater than 0.2 Å or dihedral-angle violations greater than 2°. A summary of the structural characteristics of the bucandin ensemble is given in Table 1. PROCHECK analysis [26] of the 20 structures showed that ≈ 96 % of the non-glycine and non-proline residues lay in the most favoured and 'additionally allowed' regions of the Ramachandran plot, while ≈ 3 % resided in the 'generously allowed' region. Less than 1 % of the residues lay outside the sterically allowed region of the Ramachandran plot. This was due mostly to Ala[19], which was situated in the less-defined region of the structure.

## Description of solution structure

The bucandin structure obtained in this NMR study had an overall root-mean-square deviation (RMSD) of 0.47 Å with respect to the mean structure, when the backbones of all residues in the ensemble of 20 structures were superimposed. Figure 4 summarizes the distribution of NOE constraints, RMSD and angular-order parameters for each residue in the ensemble of structures. Clearly, the overall fold is well defined, as shown by the low RMSD values of less than 0.6 Å and backbone angular order parameters greater than 0.90 for most residues. Still, some regions in the molecule were less well defined than others, as shown by their relatively higher angular order-parameter and higher local RMSD values. These included the N-terminus region up to Thr[22] and the C-terminus region from Asn[59]. As shown in Figure 4(A), the relatively low definition for the N-terminus can be ascribed to the dearth of long-range NOEs for some parts of this region. The RMSD, with respect to the mean structure, decreased to 0.24 Å when only the backbones of residues 23–58 were considered. Figure 5 shows the ensemble of 20 bucandin structures superimposed over the backbone of the well-defined region of residues 23–58. This representation clearly emphasizes the well-defined and less-defined regions of the structures as well

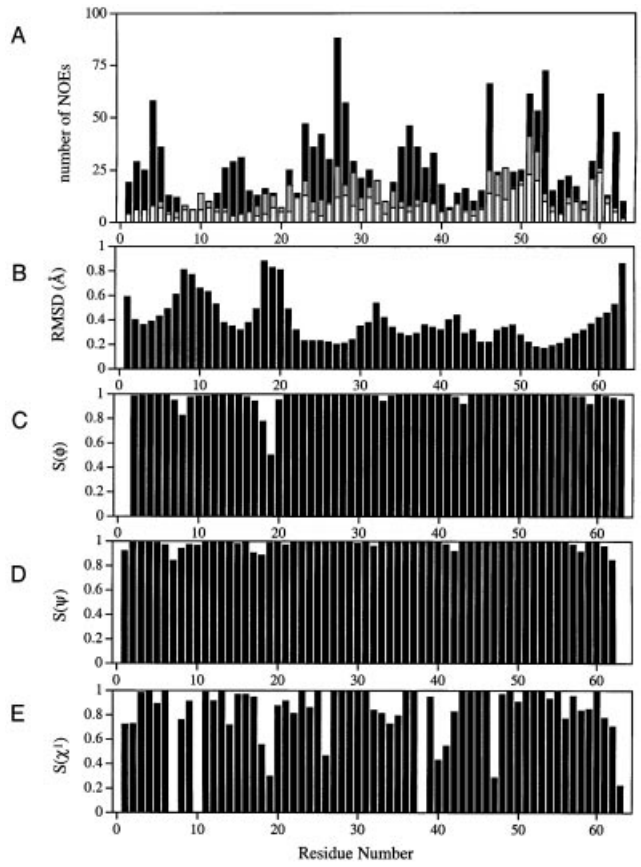


**Figure 4 Parameters characterizing the 20 structures of bucandin, plotted as a function of residue number**

(**A**) number of NOEs used in the final strucuture calculation; sequential, medium- and long-range NOEs are indicated by white, grey and black bars respectively. (**B**) RMSD from the mean structure for the backbone heavy atoms (N,C,C$\alpha$). (**C**–**E**) Angular order parameters ($S$) for the backbone ($\phi$ and $\psi$) and side-chain ($\chi^1$) dihedral angles. Gaps in the $\chi^1$ are due to Gly residues.

as the presence of three distinct loops in the molecule. The well-defined region that spans residues 23–58 incorporates two distinct loops, whereas the less defined region from the N-terminus to Thr[22] includes the other loop. It is possible that the less well-defined regions that encompass residues 1–22 and 59–63 suggest flexibilities in these parts of the molecule. This, however, cannot be verified using the NOE information alone; hence further NMR investigation on the local mobility of the bucandin is needed.

The bucandin molecule, as shown in Figure 5, adopts the typical three-finger motif of $\alpha$-neurotoxins with some peculiar structural characteristics. PROMOTIF analysis [27] of the ensemble of bucandin structures showed that the molecule incorporates two anti-parallel $\beta$-sheets with some turns, but no helix. The first sheet has two strands defined by residues 2–5 and 13–16 and is incorporated in the first of the three loops. The second sheet has four strands defined by residues 23–29, 35–40, 46–47 and 51–56; this encompasses the second and the third loop. Note that all three-finger toxins known to date have at most three strands in the second $\beta$-sheet [1–4,6]. The additional strand incorporating residues 46–47 is therefore unique to the bucandin structure. The presence of this distinct structural element was clearly supported by the NMR data, as summarized in Figure 6. The $^1$H–$^2$H exchange experiment, for example, showed that the amide of Ile[46] and Thr[48] were slow-exchanging and were therefore inferred to be hydrogen-bonded to the carbonyl group of Asn[53] and Val[51] respectively. Moreover, the chemical-shift index [28] of +1 and $^3J_{NH\alpha}$ coupling constants greater than 8 Hz for residues 46–48 also suggested that they were most likely involved in a $\beta$-strand.

The first loop in the bucandin molecule is distinct from the rest of the molecule and is orientated at an angle of $\approx 45°$ with respect to the second and third loops. This loop incorporates the first $\beta$-sheet that is twisted, and a disulphide pair that stabilize the loop. There are two kinks near the two cysteine residues, thus causing the end of the loop to be directed away from the rest of the molecule. Although the loop spanning residues 1–22 is flexible, it is well-defined locally, with an RMSD of 0.49 Å with respect to the mean structure. The turn defined by residues 18–21, situated at the base from which the three loops originate, shows a lack of definition, which implies higher mobility. The rest of the molecule, which includes the second and third loops, is probably stabilized by the four-stranded $\beta$-sheet and is therefore more rigid.

The conformations of the Cys[6]–Cys[11] and Cys[43]–Cys[55] disulphide bridges were well defined in the ensemble of 20 structures with dihedral angle $\chi_{ss}$ values of $-116\pm5°$ and $68\pm4°$. The Cys[3]–Cys[24] and Cys[17]–Cys[39] disulphide bonds were moderately well defined, with $\chi_{ss}$ values of $-131\pm35°$ and $-35\pm34°$ respectively, while that of Cys[56]–Cys[61] was poorly defined, with a $\chi_{ss}$ value of $-25\pm58°$. The lack of definition in the flexible C-terminal region is responsible for the large deviation in the $\chi_{ss}$ of the Cys[56]–Cys[61] disulphide bond.

Overall, bucandin is a relatively flat molecule, with the two anti-parallel $\beta$-sheets lying almost on the same plane (see Figure 5B). Thus it has two distinct faces, face A and face B, that are probably important for its effective interaction with its target molecule(s). The front face (face A) contains a distinct hydrophobic region near the centre, while the other face (face B) is largely positive in charge and may therefore associate with the cell membrane. The clear separation between the hydrophobic and hydrophilic portions of bucandin indicates an amphipathic molecule that may easily penetrate cell membranes and thus exert its biological effect(s) intracellularly.

## DISCUSSION

In the present study we determined the high-resolution structure of bucandin in aqueous solution. The 'quality' of the obtained structure is found to be better than many of the reported three-finger toxin solution structures to date [29–31]. This favourable outcome was primarily due to the excellent quality of its 2D NOESY spectra, which yielded numerous cross-peaks. It is therefore relevant to compare this high-quality solution structure with the recently obtained high-resolution X-ray structure and also with structures of other common three-finger toxins.

### Comparison with X-ray structure

Figure 7(A) presents the NMR and X-ray structures superimposed over the backbone atoms of all residues. Overall, the NMR structure has good correlation with the X-ray structure. An RMSD of 1.37 Å was obtained when the backbone atoms of all the residues were superimposed; this decreased to 0.94 Å when only the residues in the $\beta$-sheets were superimposed. Note that even the first loop, which shows some degree of mobility in the NMR structure, is well superimposed on the X-ray structure.

The secondary-structural elements, such as $\beta$-strands and turns, found in the crystal structure are also present in the NMR structure; however, there are differences in their extent. In the X-

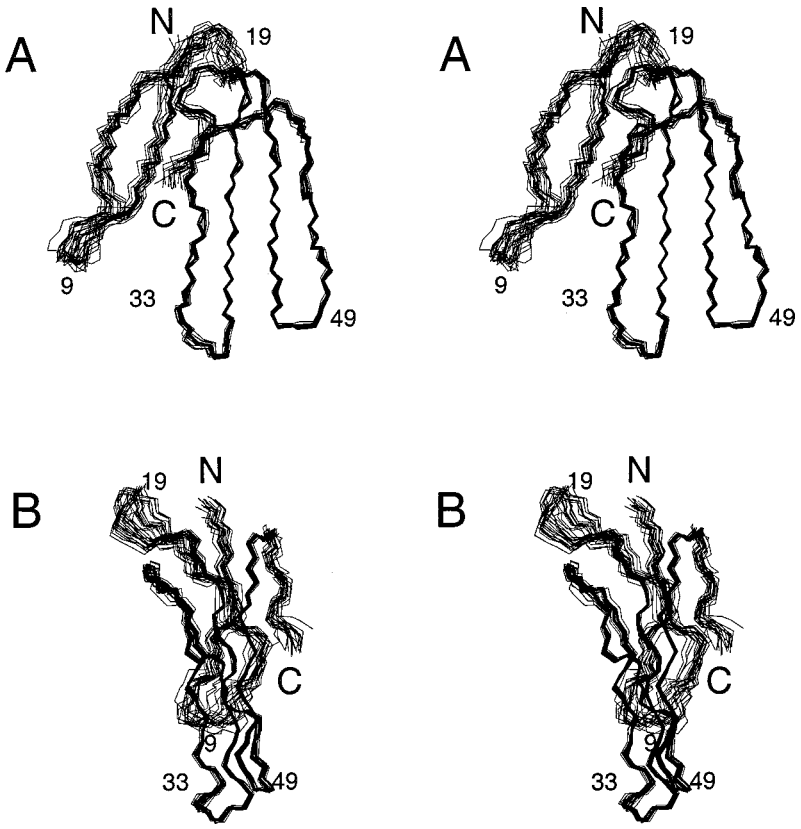


**Figure 5 Ensemble of 20 bucandin structures**

Stereo views of the ensemble of 20 bucandin structures superimposed to show the best fit over the backbone atoms of residues 23–58 of the mean co-ordinate structure. Only the N, C and C$\alpha$ atoms of the backbone are displayed. (**A**) and (**B**) are related by an $\approx 90°$ rotation about the 'virtual' vertical axis.

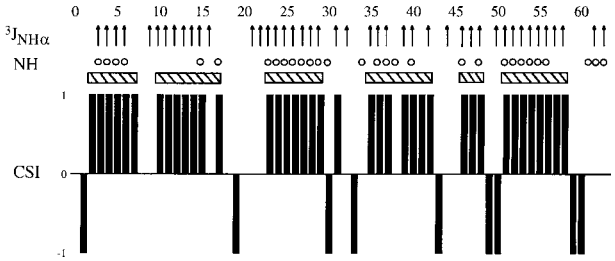


**Figure 6 Summary of NMR data for secondary structure prediction**

$^3J_{NH\alpha} > 8$ Hz are indicated by ↑. Slowly exchanging amide protons are indicated by open circles. Chemical shift indices (CSI) represented by bars are based on the deviation of the observed H$\alpha$ chemical-shift values from random-coil values [28]. Any dense grouping of 1's, such as three or more 1's uninterrupted by −1's, is suggestive of the presence of $\beta$-strand. The locations of expected $\beta$-strands in the sequence are marked by the hatched horizontal bars.

ray structure, $\beta$-strands are claimed to span residues 1–5, 13–17, 23–28, 35–39, 45–48 and 51–57, whereas, in the NMR structure, $\beta$-strands extend over residues 2–5, 13–16, 23–29, 35–40, 46–47 and 51–56. Our analysis of the X-ray structure using MOLMOL [32] showed that the extent of the second $\beta$-sheet was identical with that in the NMR structure; however, the first $\beta$-sheet was found to contain a $\beta$-bulge and was considerably longer, spanning residues 2–7 and 10–16 (see Figures 7B and 7C).

The most significant difference in the backbone fold of the two structures is situated in the region spanning residues 42–49, where an RMSD of 1.37 Å was obtained. Note that this region in the molecule includes the fourth $\beta$-strand, defined by residues 46–47, that is found to be unique to bucandin. In the NMR structure, this short strand is situated on the side of the two faces and is slightly offset from the plane defined by the three strands of the second $\beta$-sheet. In the X-ray structure, the $\beta$-strand is longer, spanning residues 45–48 and is oriented basically on the same plane as the second $\beta$-sheet [10].

Further comparisons of the solution and crystal structures also show that there are significant differences in orientations of some side chains (Figures 7B and 7C). It is clear that, although the dispositions of many of these side-chain residues are alike,

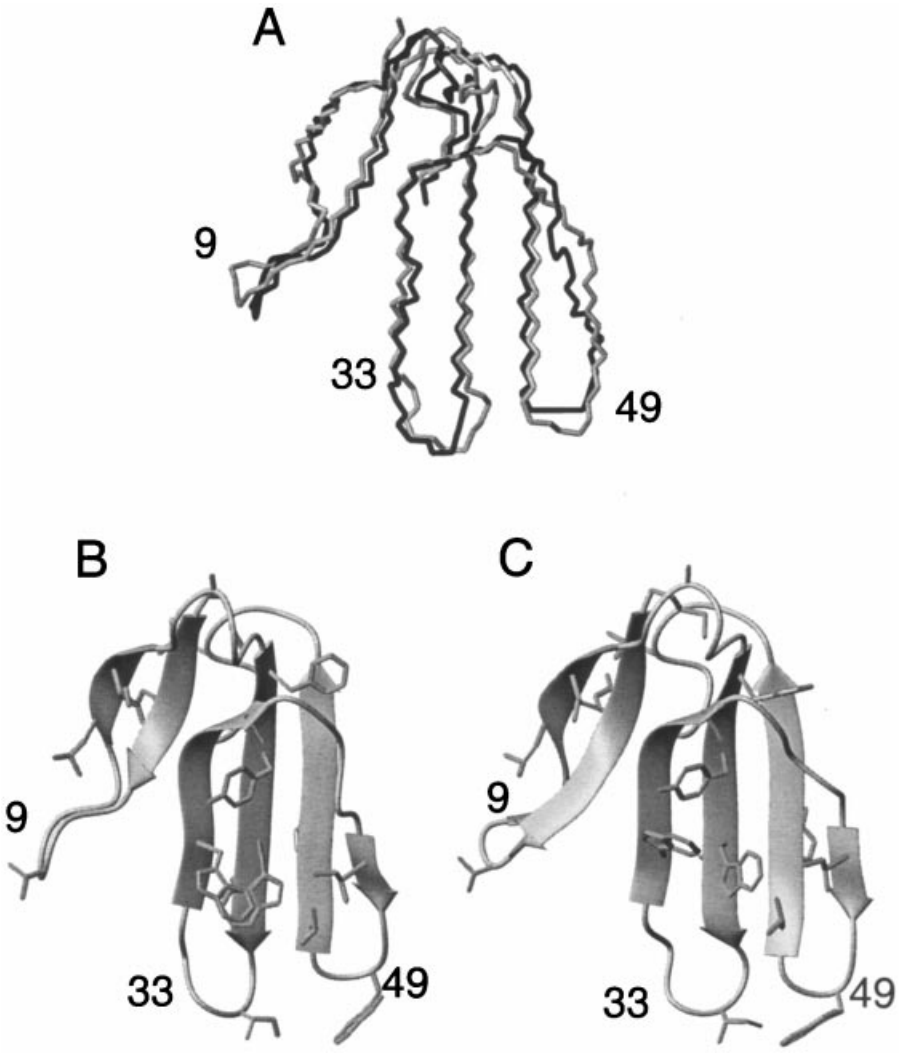


**Figure 7 Comparison of NMR and X-ray structures of bucandin**

(**A**) The two structures superimposed over N, C and Cα atoms of all backbone residues. NMR and X-ray structures are shown in black and grey respectively. (**B** and **C**) Ribbon representation of the NMR and X-ray structures respectively. The hydrophobic side chains, excluding those of cysteine residues, are shown. These Figures were drawn using the program MOLMOL [32].

those of $Trp^{27}$ and $Trp^{36}$, located on the lower portion of the middle loop, are different. These two side chains are highly defined in the NMR structures, with angular-order parameters ($\chi^1$) $\approx$ 1.0 (see Figure 4E). The side chains of $Trp^{27}$ and $Trp^{36}$ are definitely closer in the solution structure than they are in the crystal structure, so that the resulting hydrophobic patch is closer to the tip of the second loop in the NMR structure. Considering that both solution and crystal structures are of high resolution, one can surmise that the small deviations are real and are probably due to the difference in the molecular environments in which the structures were determined; these include differences in pH, temperature and the presence of intermolecular packing interactions in crystals.

## Comparison with other three-finger toxin structures

The most extensive sequence similarity between bucandin and other toxins is the 73 % similarity to S6C4, a toxin isolated from *D. j. kaimosae*. Unfortunately, little is known about this toxin's mode of action or its structure, so a detailed comparison with bucandin is not possible. The other three-finger toxins with similar five-disulphide-bond arrangements have only $\approx$ 30–40 % sequence identity with bucandin, and these include the ten cysteine residues that constitute about half of the identical residues. Since bucandin shares a similar folding pattern with these types of toxin, this suggests that the five disulphide bonds play a central role in determining and maintaining this rigid structural motif. Other similar residues which are likely to be important for the structural configuration include $^{Leu}/_{Met^1}$, $Thr^{16}$, $Glu^{21}$, $^{Phe}/_{Tyr^{25}}$, $Lys^{26}$, $Arg^{35}$, $Gly^{38}$, $Ala^{40}$, $Thr^{42}$, $^{Ser}/_{Thr^{57}}$, $Thr^{58}$, $^{Asp}/_{Asn^{59}}$ and $Asn^{62}$. In comparison with three-finger toxins that have only four disulphide bonds, conserved residues in bucandin, including $Tyr^{25}$, $Gly^{38}$, $Thr^{58}$, $Asn^{59}$ and $Asn^{62}$. $Tyr^{25}$ and $Gly^{38}$ are situated on face A at the centre of the molecule, whereas $Thr^{58}$, $Asn^{59}$ and $Asn^{62}$ are found on the C-terminus.

Figure 8 compares our calculated structure of bucandin with those of selected three-finger toxins: cobratoxin, erabutoxin and cytoxin II. The strong similarities in overall folds, as well as variations in configurations among the four molecules, are clearly highlighted in the Figure. Note that $Tyr^{25}$, situated at the centre

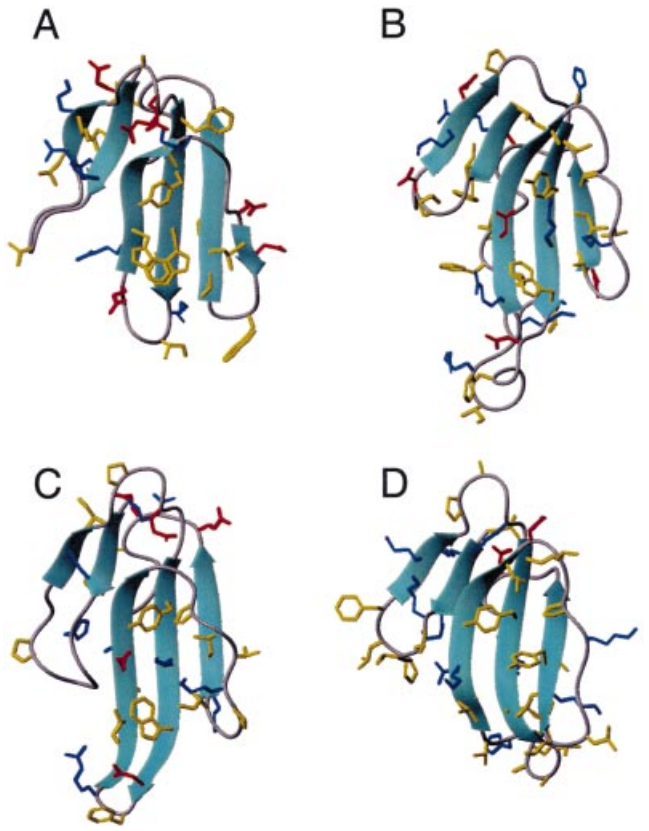


**Figure 8 Comparison of the bucandin structure with other three-finger toxins**

(**A**), bucandin; (**B**) cobratoxin (2ctx); (**C**) erabutoxin (3ebx); (**D**) cytotoxin II (1cb9). 2ctx, 3ebx, and 1cb9 refer to the Brookhaven Protein Data bank accession codes. Hydrophobic, positively and negatively charged residues are shown in yellow, blue and red respectively.

of the middle loop, is specifically conserved in the four molecules and has its side chain oriented in the same manner. The side chain of this residue is well defined in the NMR structure with $\chi^1 = 0.99$, as illustrated in Figure 4(E).

Studies on $\alpha$-neurotoxins, such as cobratoxin and erabutoxin, show that the functional residues responsible for their toxicities are situated mainly on the lower half of the second and third loops, located on the front face (face A) of the molecule [33]. The tips of the loops are flexible and usually contain some of the functionally important side chains. The upper half of the loop on the front face, on the other hand, contains a hydrophobic patch or centre, which includes a conserved tyrosine residue ($Tyr^{25}$) that is believed to be important for the stability of the antiparallel $\beta$-sheet structure.

Similar distribution patterns of structural and functional residues are seen in the cytotoxins (cardiotoxins); they contain alternating hydrophobic and hydrophilic bands that surround the molecules from the core to the tips of the loop [6]. Hydrophobic side chains, believed to be important for interaction with the lipid part of a cell membrane, occupy the tip of the three loops while the middle part, which is essentially hydrophilic, contains the structurally important tyrosine residue ($Tyr^{25}$). It is hypothesized that the composition of the tip of the second loop determines the specificity of different cytotoxins. As shown in Figure 8(A), the tips of the three loops in bucandin are not hydrophobic overall, although the tips do contain one hydrophobic residue in each loop ($Val^8$, $Ile^{31}$ and $Trp^{49}$ respectively). This structural characteristic alone suggests that bucandin is not a cytotoxin (cardiotoxin).

Even erabutoxin has a hydrophilic band in the middle of the molecule; this is similar to that found in cytotoxins, whereas cobratoxin only has a hydrophilic region in face A. It has been speculated that such a hydrophilic band, which is essentially basic, in cytotoxins could easily interact with the negatively charged surface of cell membranes [34]. The clear separation of the basic and hydrophobic parts of cytotoxins allows for a more specific interaction with membranes, which in turn causes cell disruption, leading to depolarization and cell lysis.

Bucandin does not have a hydrophilic band in the middle of its structure. There is a continuous positively charged region in face B, but this hydrophilic region is interrupted by the large hydrophobic patch in face A that is defined by $Tyr^{25}$, $Trp^{27}$, $Trp^{36}$, $Ala^{40}$, $Ile^{46}$ and $Val^{51}$. In the crystal structure, the three aromatic side chains of $Tyr^{25}$, $Trp^{27}$ and $Trp^{36}$ are almost evenly distributed, forming a continuous patch that extends the second $\beta$-sheet from $Ala^{40}$ to $Ile^{46}$. In the NMR structure, the side chains of $Trp^{27}$ and $Trp^{36}$ are stacked together and are directed towards the lower end, in essence isolated from the structurally important $Tyr^{25}$. Considering the structural and functional studies of $\alpha$-neurotoxins and cytotoxins, as mentioned above, the two Trp residues located on the lower end of the second loop are likely to be important for the activity of this toxin.

On the basis of the structure alone, it is difficult to speculate whether bucandin is an $\alpha$-neurotoxin or not, owing to the diversity of side chains found in many of these type of molecules. Note, however, that there are aspects of the bucandin structure that set it apart from other known three-finger toxin structures. The most apparent, as mentioned above, is the presence of the fourth strand, spanning residues 46–47 in the second antiparallel $\beta$-sheet. This distinct region in bucandin is highly acidic, owing to the presence of $Glu^{45}$ and $Asp^{47}$, whose side chains point outwards, towards the solvent and parallel with the plane of the molecule. On the opposite side, basic side chains of $Arg^5$, $His^{12}$ and $Lys^{14}$ are lined up along the edge of the second strand of the first $\beta$-sheet. These, together with basic residues in the middle of face B, make the bucandin molecule highly polar, with the vector of its dipole moment pointing towards the very negatively charged first loop [10].

We have presented here a high-resolution NMR structure of bucandin, a novel neurotoxin that enhances acetylcholine release from nerve terminals. The structure obtained in solution had some distinct differences from that obtained in crystals, although the overall folds are similar. The NMR study found that the first loop, which includes the two-stranded $\beta$-sheet and the C-terminus of bucandin, could probably have higher degrees of flexibility than the rest of the molecule. The low sequence similarity of bucandin with other known three-finger toxins provides useful insights into functionally and structurally important side chains in this polypeptide toxin.

This work was supported by an Australian Research Council grant to P.W.K. We thank Dr Bill Bubb and Dr Bob Chapman for help with the NMR spectrometer, and Mr Bill Lowe for expert technical assistance.

## REFERENCES

1 Smith, J. L., Corfield, P. W. R., Hendrickson, W. A. and Low, B. W. (1988) Refinement at 1.4 angstroms resolution of a model of erabutoxin B: treatment of ordered solvent and discrete disorder. Acta Crystallogr. **A44**, 357–368

2 Betzel, C., Lange, G., Pal., G. P., Wilson, K. S., Maelicke, A. and Saenger, W. (1991) The refined crystal structure of $\alpha$-cobratoxin from *Naja naja siamensis* at 2.4 Å resolution. J. Biol. Chem. **266**, 21530–21536

3 Tsetlin, V. (1999) Snake venom α-neurotoxins and other 'three-finger' proteins. Eur. J. Biochem. **264**, 281–286
4 Bilwes, A., Rees, B., Moras, D., Menez, R. and Menez, A. (1994) X-ray structure at 1.55 Å of toxin γ, a cardiotoxin from *Naja nigricollis* venom. J. Mol. Biol. **239**, 122–136
5 Wu, W. G. (1997) Diversity of cobra cardiotoxin. J. Toxicol. Toxin Rev. **16**, 115–134
6 Dementieva, D. V., Bocharov, E. V. and Arseniev, A. S. (1999) Two forms of cytotoxin II (cardiotoxin) from *Naja naja oxiana* in aqueous solution – spatial structures with tightly bound water molecules. Eur. J. Biochem. **263**, 152–162
7 Cervenansky, C., Dajas, F., Harvey, A. L. and Karlsson, E. (1991) Fasciculins, anticholinesterase toxins from mamba venoms: biochemistry and pharmacology. In Snake Toxins (Harvey, A. L., ed.), pp. 131–164, Pergamon Press, New York
8 De Weille, J. R., Schweitz, H., Maes, P., Tartar, A. and Lazdunski, M. (1991) Calciseptine, a peptide isolated from black mamba venom, is a specific blocker of the L-type calcium channel. Proc. Natl. Acad. Sci. U.S.A.. **88**, 2437–2440
9 Albrand, J. P., Blackledge, M. J., Pascaud, F., Hollecker, M. and Marion, D. (1995) NMR and restrained molecular dynamics study of the 3-D solution structure of toxin FS2, a specific blocker of the L-type calcium channel, isolated from the black mamba venom. Biochemistry **34**, 5923–5937
10 Kuhn, P., Deacon, A. M., Comoso, S., Rajaseger, G., Kini, R. M., Uson, I. and Kolatkar, P. R. (2000) The atomic resolution structure of bucandin, a novel toxin isolated from the Malayan krait, determined by direct methods. Acta Crystallogr. **D56**, 1401–1407
11 Marion, D. and Wüthrich, K. (1983) Application of phase-sensitive two-dimensional correlated spectroscopy (COSY) for measurements of $^1$H–$^1$H spin–spin coupling constants in proteins. Biochem. Biophys. Res. Commun. **113**, 967–974
12 Rance, M., Sørensen, O. W., Bodenhausen, G., Wagner, G., Ernst, R. R. and Wüthrich, K. (1983) Improved spectral resolution in COSY $^1$H NMR spectra of proteins via double quantum filtering. Biochem. Biophys. Res. Commun. **117**, 479–465
13 Derome, A. E. and Williamson, M. P. (1990) Rapid-pulsing artifacts in double-quantum-filtered COSY. J. Magn. Reson. **88**, 177–185
14 Griesinger, C., Sørensen, O. W. and Ernst, R. R. (1987) Practical aspects of the E.COSY technique. Measurement of scalar spin–spin coupling constants in peptides. J. Magn. Reson. **75**, 474–492
15 Bax, A. and Davis, D. G. (1985) MLEV-17 based two-dimensional homonuclear magnetisation transfer spectroscopy. J. Magn. Reson. **65**, 355–360
16 Kumar, A., Ernst, R. R. and Wüthrich, K. (1980) A two-dimensional nuclear Overhauser enhancement (2D nOe) experiment for elucidation of complete proton-proton cross-relaxation networks in biological macromolecules. Biochem. Biophys. Res. Commun. **95**, 1–6
17 Piotto, M., Saudek, V. and Sklenár, V. (1992) Gradient-tailored excitation for single-quantum NMR spectroscopy of aqueous solutions. J. Biomol. NMR **2**, 661–665
18 Bartels, C., Xia, T., Billeter, M., Güntert, P. and Wüthrich, K. (1995) The program XEASY for computer-supported NMR spectral analysis of biological macromolecules. J. Biomol. NMR. **5**, 1–10
19 Szyperski, I., Güntert, P., Otting, G. and Wüthrich, K. (1992) Determination of scalar coupling constants by inverse Fourier transformation of in-phase multiplets. J. Magn. Reson. **99**, 552–560
20 Wagner, G., Braun, W., Havel, T. F., Schaumann, T., Gō, N. and Wüthrich, K. (1987) Protein structures in solution by nuclear magnetic resonance and distance geometry. The polypeptide fold of the basic pancreatic trypsin inhibitor determined using two different algorithms, DISGEO and DISMAN. J. Mol. Biol. **196**, 611–639
21 Mumenthaler, C. and Braun, W. (1995) Automated assignment of simulated and experimental NOESY spectra of proteins by feedback filtering and self-correcting distance geometry. J. Mol. Biol. **254**, 465–480
22 Mumenthaler, C., Güntert, P., Braun, W. and Wüthrich, K. (1997) Automated combined assignment of NOESY spectra and three-dimensional structure determination. J. Biomol. NMR **10**, 351–362
23 Güntert, P., Mumenthaler, C. and Wüthrich, K. (1997) Torsion angle dynamics for NMR structure calculation with the new program DYANA. J. Mol. Biol. **273**, 283–298
24 Brünger, A. T. (1992) X-PLOR Version 3.1. A System for X-ray Crystallography and NMR, Yale University, New Haven
24a Torres, A. M., de Plater, G. M., Doverskog, M., Birinyi-Strachan, L. C., Nicholson, G. M., Gallagher, C. H. and Kuchel, P. W. (2000) Defensin-like peptide-2 from platypus venom: member of a class of peptides with a distinct structural fold. Biochem. J. **348**, 649–656
25 Wüthrich, K. (1986) NMR of Proteins and Nucleic Acids, John Wiley and Sons, New York
26 Laskowski, R. A., MacArthur, M. W., Moss, D. S and Thorton, J. M. (1993) PROCHECK: a program to check the stereochemical quality of protein structure coordinates. J. Appl. Crystallogr. **26**, 283–292
27 Hutchinson, E. G. and Thorton, J. M. (1996) PROMOTIF – a program to identify and analyze structural motifs in proteins. Protein. Sci. **5**, 212–220
28 Wishart, D. S., Sykes, B. D. and Richards, F. M. (1992) The chemical shift index: a fast and simple method for the assignment of protein secondary structure through NMR spectroscopy. Biochemistry **31**, 1647–1651
29 Peng, S. S., Kumar, T. K., Jayaraman, G., Chang, C. C. and Yu, C. (1997) Solution structure of toxin b, a long neurotoxin from the venom of the king cobra (*Ophiophagus hannah*). J. Biol. Chem. **272**, 7817–7823
30 Connolly, P. J., Stern, A. S. and Hoch, J. C. (1996) Solution structure of LSIII, a long neurotoxin from the venom of *Laticauda semifasciata*. Biochemistry **35**, 418–426
31 Ségalas, I., Roumestand, C., Zinn-Justin, S., Gilquin, B., Ménez, R., Ménez, A. and Toma, F. (1995) Solution structure of a green mamba toxin that activates muscarinic acetylcholine receptors, as studied by nuclear magnetic resonance and molecular modeling. Biochemistry **34**, 1248–1260
32 Koradi, R., Billeter, M. and Wüthrich, K. (1996) MOLMOL: a program for display and analysis of macromolecular structures. J. Mol. Graph. **14**, 51–55
33 Endo, T. and Tamiya, N. (1991) Structure–function relationships of postsynaptic neurotoxins from snake venoms. In Snake Toxins (Harvey, A. L., ed.), pp. 165–222, Pergamon Press, New York
34 Dufourcq, J., Faucon, J. F., Bernard, E., Pezolet, M., Tessier, M., Bougis, P., van Rietschoten, J., Delori, P. and Rochat, H. (1982) Structure–function relationships for cardiotoxins interacting with phospholipids. Toxicon. **20**, 165–174

Received 4 July 2001/23 August 2001; accepted 8 October 2001